SYNTHESIS, MICROSTRUCTURE AND HARDNESS OF FUNCTIONALLY GRADED HYDROXYAPATITE/Co-Cr-Mo (F75) PREPARED USING POWDER METALLURGY

N. AB LLAH, S. B. JAMALUDIN[*], N. H. AHMAD ZAIDI,
Z. A. ZAHID JAMAL
*Sustainable Engineering Research Cluster, School of Materials Engineering,
University Malaysia Perlis, 01000 Kangar, Perlis, Malaysia*

Human bone consists of graded structure which is more compact in the outer layer and porous inside the bone. This structure ensures blood circulation occur inside the bone and also sustains high impact load throughout the bone activity. In this research, functionally graded of hydroxyapatite (HAP) and Co-Cr-Mo (F75) was synthesised using powder metallurgy to imitate the natural bone. Three layers of graded structures were synthesised based on first layer was the 100wt% HAP, intermediate layer was the mixture of HAP and F75, finally third layer was the 100wt% F75. The effect of composition in the intermediate layer was studied by varying the weight percentage of HAP and F75 in the intermediate layer. Microstructure and hardness behaviour were investigated. The finding showed that pores and microcrack present as the content of HAP increased in the intermediate layer. Energy Dispersive Spectroscopy (EDS) analysis showed that the diffusion of calcium, cobalt, chromium and molybdenum occurred during sintering process. Hardness value indented on the intermediate layer increased as the percentage of HAP increased.

1. Introduction

Functionally graded material (FGM) is a new material which it properties vary gradually with position depends on chemical composition, microstructure or atomic order [1]. Functionally graded materials can be synthesized using powder metallurgy technique, plasma spray coating, physical vapour deposition (PVD), chemical vapour deposition (CVD), electro-deposition and centrifugal casting method [2]. Plasma spray coating, PVD and CVD technology are high cost fabrication techniques and also prone to in-homogeneities, oxide inclusion and porosity in the coating during the coating formation [3]. Casting techniques are difficult to produce a complex shape. More advantages have been offered by powder metallurgy technique such as materials utilization, shape complexity, near net shape dimensional control and also low cost [4]. Research on fabrication and development of FGM has grown drastically due to the demand for the materials that can satisfy more than one property. Recently, the application of functionally graded materials in biomedical is inspired by the nature of the bone which is can be imitated by FGM.

Human bones have a functional gradation structure which changes from dense in the external and porous in the internal part of the bones [5].

Several researchers have synthesised and characterised functionally graded materials for biomedical applications. Watari et al. [6] investigated the tissue reaction to the gradient composition of the functional graded titanium/HAP and titanium/cobalt. The result showed that there is a possibility to control the tissue response by the functional graded structure. Thieme et al. [7] synthesised a skeletal system of the porosity graded material to achieve elastic modulus value

---

up to the level of the cortical bone. Tampieri et al. [8] have used hydroxyapatite to fabricate the porosity graded structure with the aim to simulate bone tissue morphology. No study available on the FGM of HAP and Co-Cr-Mo alloy, therefore this work was aimed to synthesis the functional graded HAP/Co-Cr-Mo by powder metallurgy and to investigate the microstructure at the interface and its hardness. HAP and Co-Cr-Mo alloy were because they are commonly used as implant materials in biomedical application.

2. Experimental procedures

2.1. Raw Materials and Preparation

The raw materials used in this research were ready-mixed Co-Cr-Mo (F75) powder supplied by the Sandvik Osprey, Australia and hydroxyapatite (HAP) powder from the Berkeley Advanced Biomaterials Inc. Particle size of raw materials was analysed using the MALVERN particle size analyser. Figure 1 shows the result for the mean size of F75 is 13.18 µm while Figure 2 shows the mean size of HAP powder is 7.59 µm.
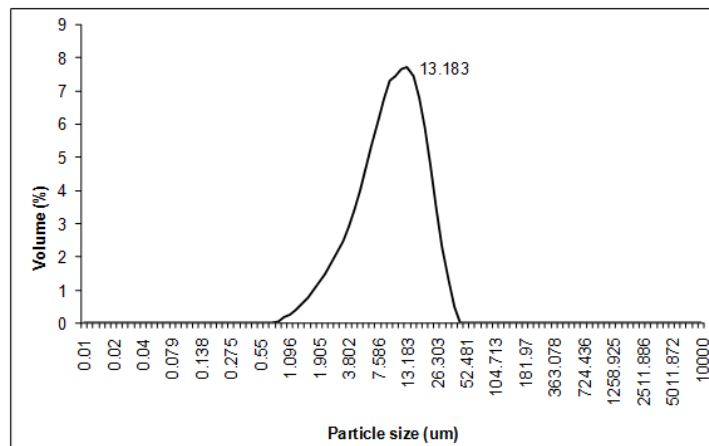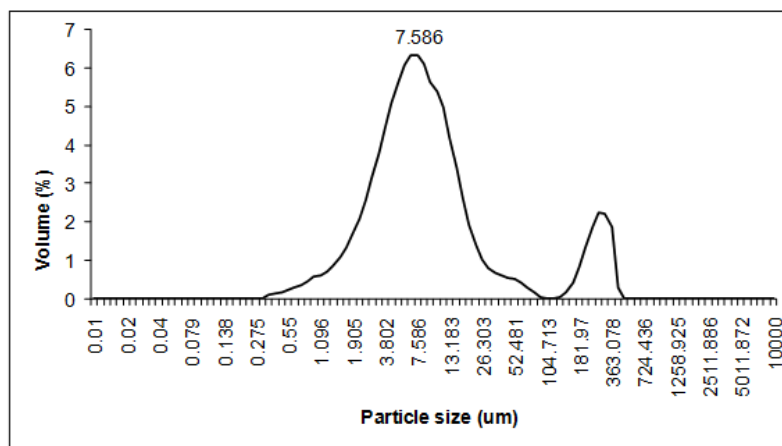

Fig. 1 Particle size of F75

Fig. 2 Particle size of HAP

Fig. 3 displays the morphology of Co-Cr-Mo powder is spherical shape. HAP powder was also observed under a scanning electron microscope (SEM) indicating the morphology of flake shape as displayed in Fig. 4.
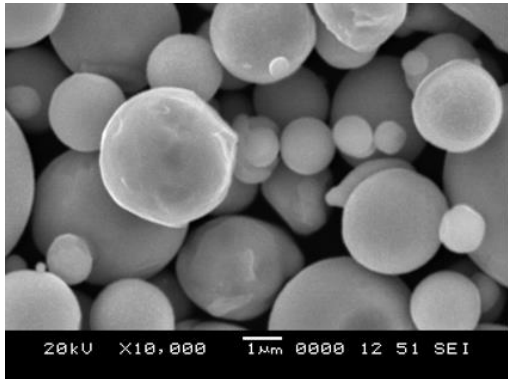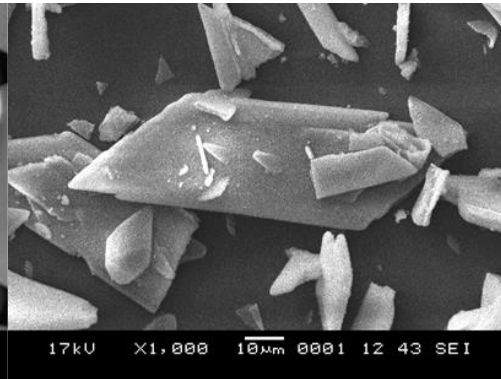
Fig. 3 SEM micrograph of F75 powder

Fig. 4 SEM micrograph of HAP powder

F75 and HAP powders were weighed according to the designed ratio and mixed mechanically using a roll mill to make them homogeneous. The mixed powders were stacked layer by layer in the die according to the pre-designed composition as illustrated in Fig. 5.

Fig. 5 Schematic diagrams of the layers according to
design composition in samples A, B, C, D, E and F

A single punch hydraulic compaction press was used to compact the compositions powder into green compacts. All samples were compacted at 500 MPa followed by sintering at 1250ºC in a tube furnace under Argon atmosphere.

2.2. Characterization

Samples were characterized using Vickers microhardness test and Scanning Electron Microscope (SEM) with energy dispersive spectroscopy (EDS). For SEM observation, sintered sample was cut using a diamond precision cutter in order to observe the cross sectional area then polished according to the standard preparation for microstructural examination.

3. Results and discussion

3.1. Physical Appearance Before and After Sintering Process

Fig. 6 shows the physical appearance of sample A, which has 25wt% HAP/75wt% F75 in the intermediate layer before and after sintering process. The appearance of cone shape after sintering process is due to the different rate of shrinkage. The layer contains 100wt% HAP shows higher shrinkage than 100wt% F75 layer. Smaller particles of HAP contribute to the higher shrinkage compare to larger particles of F75. Different type of particles that have different properties and phase also contributes to the shrinkage rate mismatch between the layers.
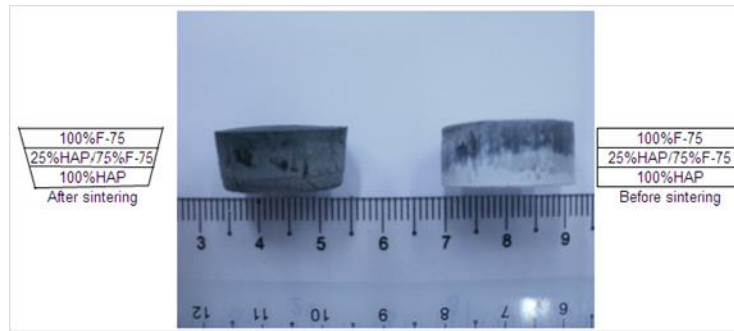
Fig 6 shows photograph of sample A before and after sintering

3.2. Microstuctural analysis

Figs. 7 and 8 indicate the microstructure of F75 and HAP green compact before sintering respectively. Smaller powder of F75 fills up the space between large powders. Generally, the smaller powder can reduce the formation of pores inside the sintered samples. SEM micrograph of HAP green compact shows the powders are stacked homogenously indicating very close arrangement of particles. There are no visible pores observed in the green compact of HAP. Flaky shape of HAP is easier to bond together compare to spherical shape [9].
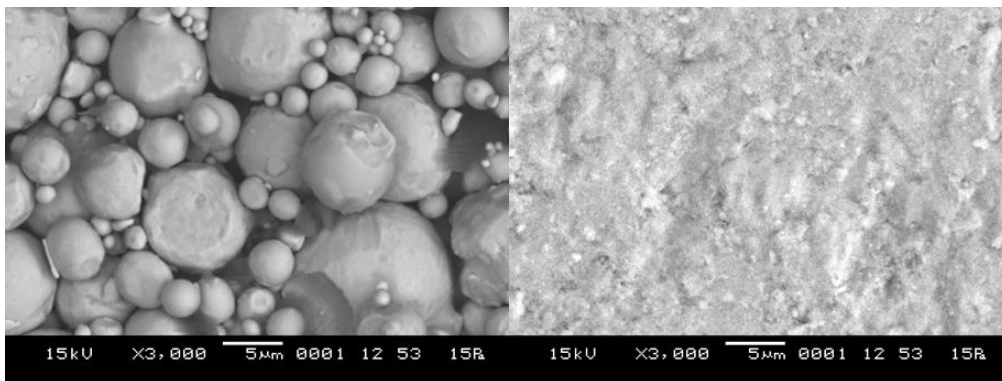

Fig. 7 SEM of F75 green compact   *Fig. 8 SEM of HAP green compact*

Fig. 9 (a-f) represents the micrograph of cross section of the sintered samples A, B, C, D, E and F indicating the physical bonding between the layers. The first layer is 100wt% HAP while the third layer is 100% F75. The intermediate layer is added in order to reduce the properties mismatch between the ceramic (100wt% HAP) and metal (100wt% F75). The intermediate layer of sample A, B, C, D, E and F is 25wt% HAP/75wt% F75, 35wt% HAP/65wt% F75, 45wt% HAP/55wt% F75, 55wt% HAP/45wt% F75, 65wt% HAP/35wt% F75 and 75wt% HAP/25wt% F75 respectively. The result shows that the variation of composition has changed the microstructure of sintered samples from 100wt% HAP to 100wt% F75. The interface microstructure between different layers can give information about the bonding strength between the layers. Sample E shows a fine crack at the interface between intermediate layer and third layer. This micro-crack propagates parallel to the layer along the boundary of the intermediate layer and third layer. This observation indicates less relaxation of residual stress and affects the physical bonding of the layers. Similar observation was reported for the functionally graded WC/Mo [10]. In addition, the microstructure of sample E also has a large crack propagates perpendicular to the layer of 100wt% HAP (first layer). Micrograph of sample D indicates the third layer is the thinnest layer than other samples. This kind of structure occurs because the third layer flakes off during the cutting process. In general, the result shows that the thickness of the intermediate layer increases from sample A to F because of the increasing content of HAP.
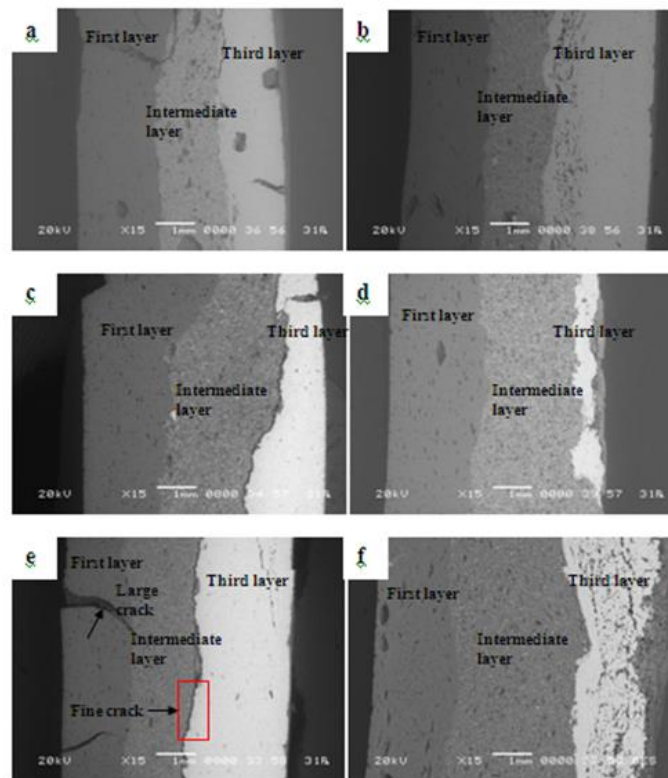
Fig. 9 Microstructure of cross section of sintered samples (a) A (b) B
(c) C (d) D (e) E and (f) F

Fig. 10 (a-f) represents microstructures of the third layer and the intermediate layer at high magnification. Samples A and B have the most stable interface layer created after the sintering process while the most visible crack can be observed at the interface of samples E and F. The dislocation density in metallic component increases with the increasing content HAP in the graded layers [11]. Another reason is the additional microscopic stress is developed the metallic component due the elastic mismatches between the metal and ceramic phase. This microscopic stress may contribute crack in the sample [12]. The mismatch of shrinkage rate also contributes to the crack existence at the interface. Therefore, samples E and F have the large mismatch to generate cracks at the interface of third layer and intermediate layer that consists of 75wt% HAP/25wt% F75 and 65wt% HAP/35wt% F75 respectively. During sintering process, the two different materials may shrink with different rates, which lead to the development of mismatch stress and generate interfacial de-bonding or part cracking at the interface [13]. Mismatch stress also can be developed due to the differences of densification kinetics and thermal expansion that presence at different level of sintering stage. Both types of mismatch stresses can contribute to the formation of defects in the FGM sintered body [14].
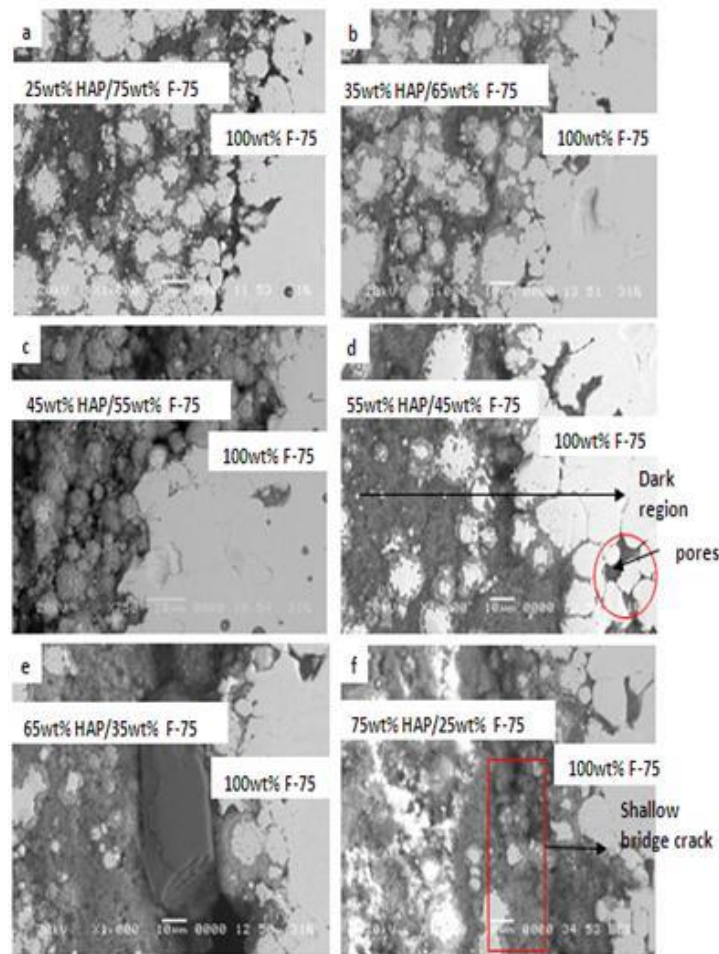
Fig. 10 Microstructures of interface between third layer and intermediate layer
of samples (a) A (b) B (c) C (d) D (e) E and (f) F at magnification

Fig. 11(a-f) shows the microstructure of interface between the first layer (100wt% HAP) and the intermediate layer. There is no significant crack occurs at the interface for all samples. It seems that the third layer (100wt% F75) layer is more prone to develop crack compare to first layer (100wt% HAP). However, as the content of HAP in the intermediate layer increases from sample A to F, the interface could not be observed clearly. The distinct interface can be observed in the sample A. Figure 12 shows EDS analysis of first layer at point 033 (100wt% HAP) for sample A indicating the presence of Cr, Co and Mo elements, whereas analysis of the intermediate layer (point 034 and 035) indicating the presence of calcium. This is the evidence of diffusion that occurs during the sintering process to bond the HAP and F75 powder.
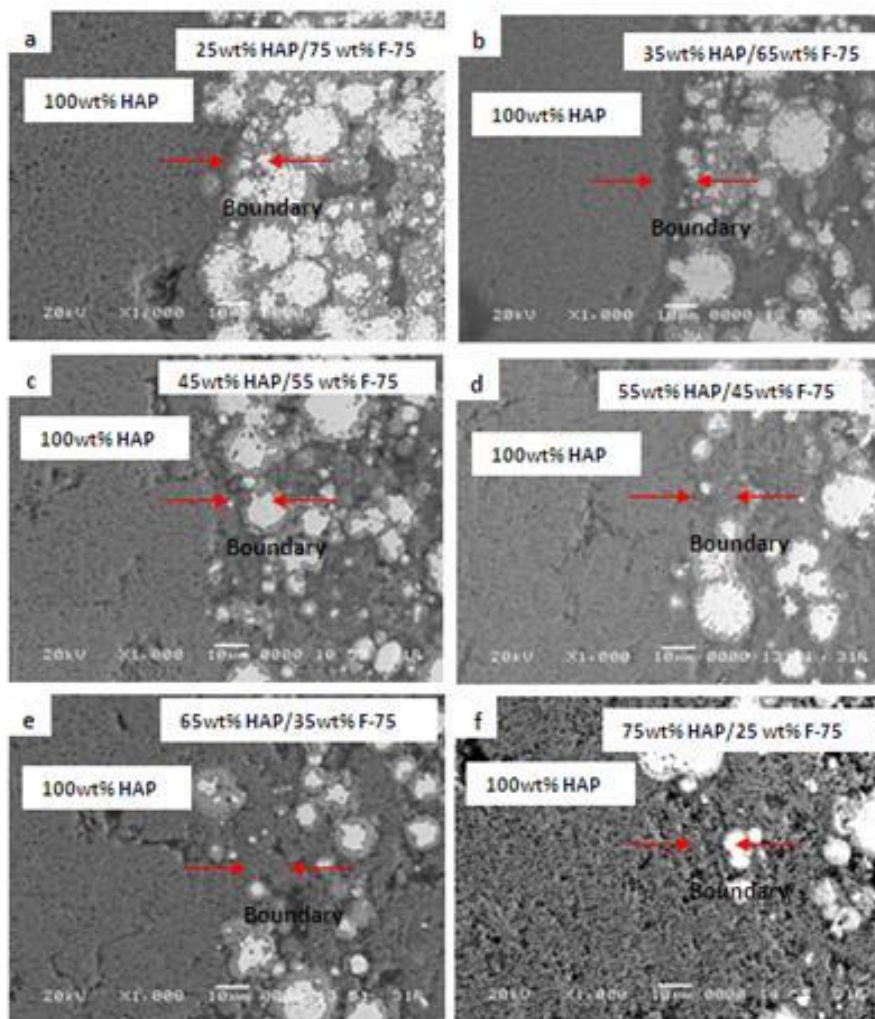
Fig. 11 Microstructures of interface between first layer and intermediate layer of samples
(a) A (b) B (c) C (d) D (e) E and (f) F at magnification

033		
Element	Mass%	At %
Ca	51.16	81.49
Cr	6.82	4.19
Co	11.82	12.81
Mo	2.28	1.52

034		
Element	Mass%	At %
Ca	1.82	3.64
Cr	9.26	7.15
Co	64.97	88.48
Mo	0.87	0.73

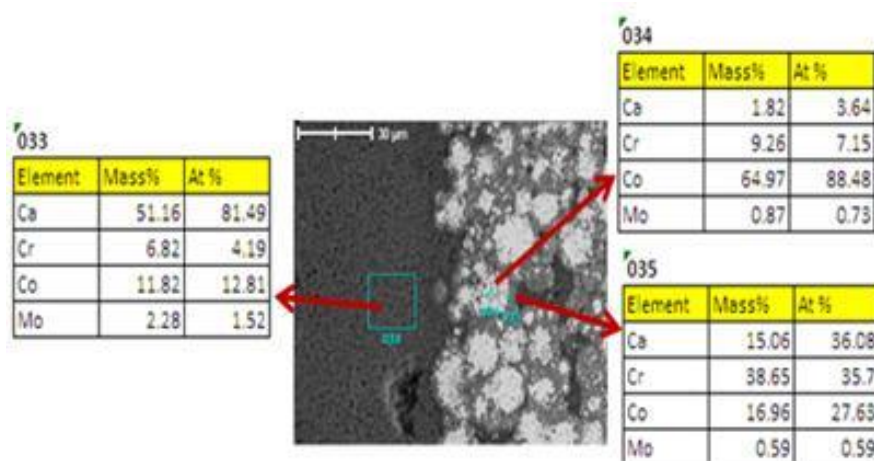| 035		
Element	Mass%	At %
Ca	15.06	36.08
Cr	38.65	35.7
Co	16.96	27.63
Mo	0.59	0.59

Fig. 12 SEM micrograph at the interface layer for sample A (intermediate layer
of 25wt% HAP/75wt% F75) with energy dispersive spectroscopy (EDS) analysis

Three elements which are calcium, chromium and cobalt in the selected sample (sample F) are mapped using the EDS analysis as illustrated in Figure 13. From this mapping, calcium,

chromium and cobalt is represented by the red, green and blue colour respectively. In the third layer (100wt% F75), calcium element can be detected. Chromium can be seen accumulated alongside the interface and also segregated around cobalt.
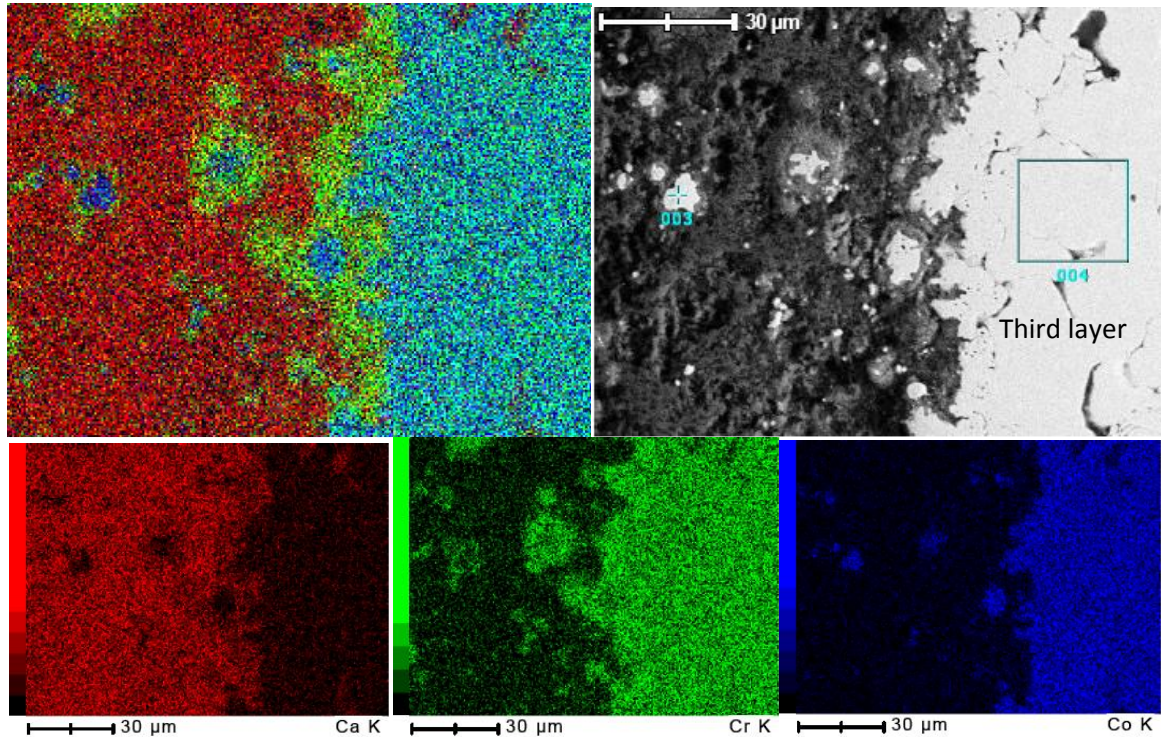

Fig. 13 Mapping of calcium, chromium and cobalt distribution by EDS in sample F

3.2. Hardness of the sintered samples

Fig. 14 shows the hardness value of the intermediate layer for samples A to F. The hardness value increases as the content of HAP increases in the intermediate layer. This result can be correlated with the properties of sintered HAP as a ceramic which is harder than sintered F75. It can be evidenced by observing the hardness of sintered 100wt% HAP and 100wt% F75 as shown in Figure 15. The hardness of 100wt% HAP is harder (164.2 Hv) than F75 which is 93.5 Hv. The addition of HAP in the F75 makes the sample harder in the intermediate layer. Chenglin et al. [11] also reported the similar result, which is hardness increased with the increasing content of HAP in the functional graded HAP/Ti. The value of hardness increased according to the rules of mixtures. Besides, the diffusion process may also increase the bonding strength of sample.
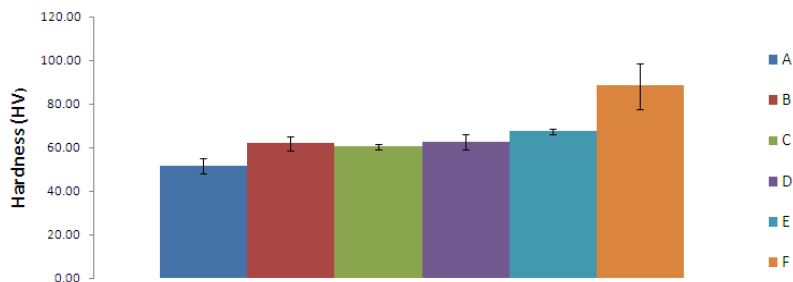

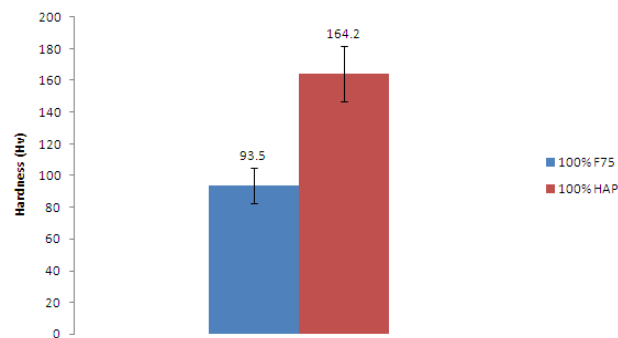*Fig. 14 Microhardness value of the intermediate layer of the samples*

Fig. 15 Microhardness value of sintered 100wt% F-75 and 100wt% HAP

4. Conclusions

Functionally graded HAP/F75 can be synthesised by powder metallurgy. Microstructural analysis shows that pores and microcrack can be produced if the content of HAP is increased in the intermediate layer. Thermal expansion mismatch of HAP and F75 and shrinkage rate difference leads to this situation. This method can be used to imitate the structure of human bone. The hardness of the intermediate layer increases as the content of HAP increases. This is related to the hardness of sintered HAP is higher than sintered F75. The EDS mapping result shows that the diffusion of elements of raw materials occurs during sintering and may increase the bonding strength of the samples.

Acknowledgements

References

[1] B. Kieback, A. Neubrand, H. Riedel, Materials Science and Engineering: **A, 362,** 81 (2003)

[2] Y. Watanabe, Y. Inaguma, H. Sato, E. M. Fujiwara, Materials, **2**, 2510 (2009)

[3] H. S. Kim, H. H. Yang, I. H. Oh, S. S. Kim, Materials Science Forum, **308-311**, 226 (1999)

[4] A. R. Khoei, R. W. Lewis, Finite Element in Analysis and Design, **30**, 335 (1998)

[5] W. Pompe, H. Worch, M. Epple,W. Friess, M. Gelinsky, P. Greil, et al., Materials Science and Engineering, **362**, 40 (2003)

[6] F. Watari, A. Yokoyama, F. Saso, M. Uo, T. Kawasaki, Materials Science Forum **308-311,** 356 (1999)

[7] M. Thieme, K. P. Wieters, F. Bergner, D. Schwarnweber, H. Worch, J. Ndop, et al. Materials Science Forum, **308-311**, 374 (1999)

[8] A. Tampieri, G. Celotti, S. Sprio, A. Delcogliano, S. Franzese, Biomaterials, **22(11)**,1365 (2001)

[9] R. M. German, Powder Metalurgy Science, Powder Industries Federation, New Jersey (1994)

[10] M Omori, T. Kakita, A. Okubo, T. Hirai, Materials Science Forum, 308-311, 53 (1999)

[11] C. Chenglin, Z. Jingchuan, Y. Zhongda, W. Shidong, Materials Science and Engineering: A, **271**, 95 (1999)

[12] V. Birman, L. W. Byrd, Applied Mechanics Review, **60,** 195 (2007)

[13] M. Dourandish, D. Godlinski, A. Simchi, V. Fiouzdor, Materials Science and Engineering, **472**, 338 (2008)

[14] B. Zhang, M. M. Gasik, Computational Materials Science, **25**, 264 (2002)